# An NAADP-gated Two-pore Channel Targeted to the Plasma Membrane Uncouples Triggering from Amplifying Ca²⁺ Signals*[S]

**Eugen Brailoiu**[‡1], **Taufiq Rahman**[§1,2], **Dev Churamani**[¶], **David L. Prole**[§3], **G. Cristina Brailoiu**[‡], **Robert Hooper**[¶4], **Colin W. Taylor**[§5], and **Sandip Patel**[¶6]

*From the* ‡*Department of Pharmacology, Temple University School of Medicine, Philadelphia, Pennsylvania 19140, the* §*Department of Pharmacology, Cambridge University, Cambridge CB2 1PD, United Kingdom, and the* ¶*Department of Cell and Developmental Biology, University College London, London WC1E 6BT, United Kingdom*

**Nicotinic acid adenine dinucleotide phosphate (NAADP) is a ubiquitous messenger proposed to stimulate Ca²⁺ release from acidic organelles via two-pore channels (TPCs). It has been difficult to resolve this trigger event from its amplification via endoplasmic reticulum Ca²⁺ stores, fuelling speculation that archetypal intracellular Ca²⁺ channels are the primary targets of NAADP. Here, we redirect TPC2 from lysosomes to the plasma membrane and show that NAADP evokes Ca²⁺ influx independent of ryanodine receptors and that it activates a Ca²⁺-permeable channel whose conductance is reduced by mutation of a residue within a putative pore. We therefore uncouple TPC2 from amplification pathways and prove that it is a pore-forming subunit of an NAADP-gated Ca²⁺ channel.**

Nicotinic acid adenine dinucleotide phosphate (NAADP) [7] is a potent Ca²⁺-mobilizing messenger in many cells, where it regulates processes as diverse as fertilization and neuronal growth (1). Recent studies suggest that ubiquitous but poorly characterized ion channels, the two-pore channels (TPCs), are credible candidates for the NAADP receptor (2–7). Localiza-tion of TPCs to the endo-lysosomal system and modification of NAADP-evoked Ca²⁺ signals after changes in TPC expression (2–6) support the idea that TPCs mediate NAADP-evoked Ca²⁺ signals from acidic organelles (8–12). But the Ca²⁺ signals evoked by NAADP are often attenuated when Ca²⁺ release from the endoplasmic reticulum (ER) is inhibited (11–16), leading some to suggest that the initial NAADP-evoked Ca²⁺ signal is amplified by ryanodine or inositol trisphosphate receptors (Fig. 1*A*, *i* and *ii*) (10–14) and others to conclude that ryanodine receptors are the primary targets of NAADP (Fig. 1*Aiii*) (15, 17–19). It has proven difficult to observe NAADP-mediated Ca²⁺ signals free of their presumed interactions with conventional intracellular Ca²⁺ channels in the ER. The inaccessibility of intracellular NAADP-sensitive channels to patch clamp recording has further limited opportunities to resolve directly their biophysical properties. Here, we address these issues by mutating a lysosomal targeting sequence in TPC2. This redirects TPC2 to the plasma membrane, where it is both uncoupled from ryanodine receptors and accessible to electrophysiological analysis.

## EXPERIMENTAL PROCEDURES

*Plasmids*—Plasmids encoding wild-type mRFP- and GFP-tagged TPC1 and TPC2 were described previously (4). A construct encoding human TPC1 lacking residues 3–12 (TPC1ΔN) was generated by PCR using the primers 1F and 1R and IMAGE clone 40148827 (accession number BC150203) as template. Primer sequences are presented in supplemental Table S1. The product was cloned into pCS2+GFP or pCS2+mRFP (described in Ref. 4) at the ClaI and EcoRI sites to introduce the fluorescent tag at the C terminus. TPC2 lacking residues 3–25 (TPC2ΔN) was generated using the primers 2F and 2R and IMAGE clone 5214862 (accession number: BC063008). The product was cloned into the EcoRI and XhoI sites. Constructs in which Leu-740 and Leu-741 of TPC1 were replaced by Ala were generated by sequence overlap extension using the mutagenic primers 3F and 3R and the outer primers 4F and 1R. The cassette was digested with BspEI and EcoRI and cloned into the corresponding sites of pCS2+TPC1 mRFP or pCS2+TPC1ΔN mRFP to generate constructs encoding mRFP-tagged TPC1[AA] or TPC1ΔN[AA]. Constructs in which Leu-11 and Leu-12 of GFP-tagged or mRFP-tagged TPC2 were replaced by Ala (TPC2[AA]) were generated using the QuikChange® Site-di-

[1] Both authors contributed equally to this work.
[2] Research Fellow of Pembroke College, Cambridge.
[3] Meres Senior Research Associate of St. John's College, Cambridge.
[4] Recipient of a Ph.D. studentship from the Biotechnology and Biological Sciences Research Council.
[5] To whom correspondence may be addressed: Dept. of Pharmacology, Tennis Court Rd., Cambridge CB2 1PD, United Kingdom. E-mail: cwt1000@cam.ac.uk.
[6] To whom correspondence may be addressed: Dept. of Cell and Developmental Biology, Gower St., London, WC1E 6BT, United Kingdom. E-mail: patel.s@ucl.ac.uk.

[7] The abbreviations used are: NAADP, nicotinic acid adenine dinucleotide phosphate; BisTris, bis(2-hydroxyethyl)iminotris(hydroxymethyl)methane; ER, endoplasmic reticulum; γ, single-channel conductance; HEK, human embryonic kidney; NMDG, *N*-methyl-D-glucamine; $NP_o$, mean channel activity; $NP_o$, basal activity; $P_o$, single-channel open probability; pS, picosiemens; RFP, red fluorescent protein; TIRF, total internal reflection fluorescence; TPC, two-pore channel.
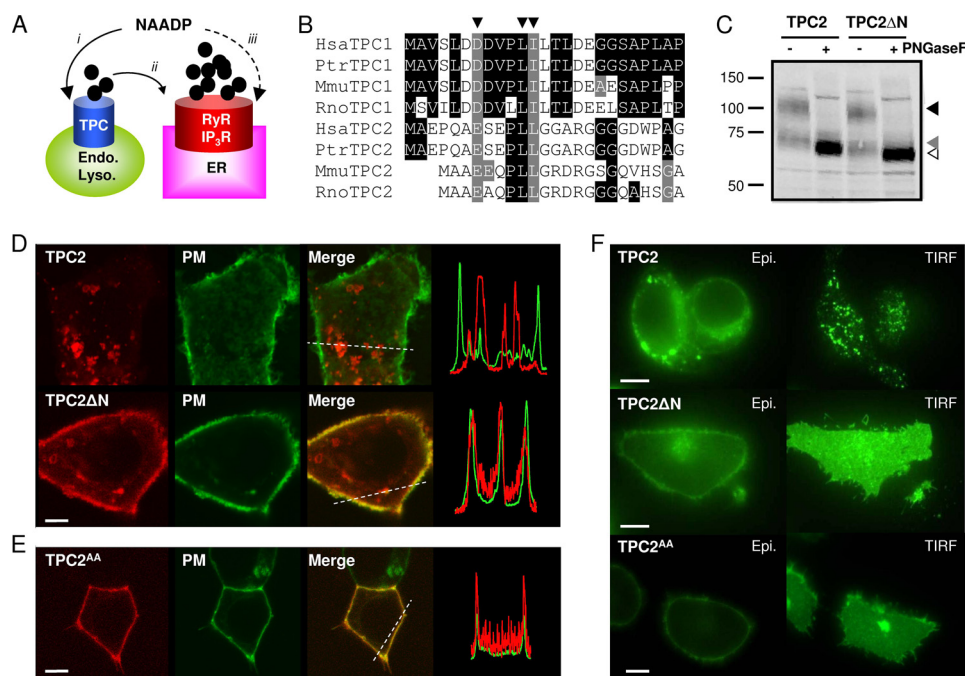
FIGURE 1. **Removal of the N terminus redirects TPC2 from lysosomes to the plasma membrane.** *A*, possible actions of NAADP. NAADP is proposed to activate TPCs on the endo-lysosomal system (*i*) followed by amplification of these trigger signals by ER $Ca^{2+}$ channels (*ii*) such as ryanodine receptors (RyR) and inositol trisphosphate receptors ($IP_3R$). Alternatively, NAADP has been proposed to activate $Ca^{2+}$ release from the ER directly (*iii*). *B*, sequence alignments of Human (*Hsa*), chimpanzee (*Ptr*), mouse (*Mmu*) and rat (*Rno*) TPC N-terminal sequences highlighting a conserved dileucine endo-lysosomal targeting motif conforming to the consensus sequence (DE)*XXX*L(L/I) (*arrowheads*). *C*, Western blot analysis of SKBR3 cell extracts expressing GFP-tagged TPC2 or TPC2ΔN (10 $\mu$g/lane). Samples were incubated with (+) or without (−) peptide:*N*-glycosidase F (*PNGaseF*) prior to analysis. *Arrowheads* mark the positions of fully glycosylated (*black arrowhead*), core glycosylated (*gray arrowhead*), and deglycosylated (*white arrowhead*) TPC2 or TPC2ΔN. Results are representative of three experiments. *D*, confocal fluorescence images of SKBR3 cells coexpressing GFP-tagged human reduced folate carrier to delineate the plasma membrane (*PM*) and either mRFP-tagged TPC2 (*top*) or mRFP-tagged TPC2 lacking residues 3–25 (TPC2ΔN; *bottom*). Merged images are overlays of the plasma membrane marker (*green*) and TPC constructs (*red*). Transect analyses of *red* and *green* fluorescence intensities across the regions marked by *dotted lines* are shown on the *right*. *E*, confocal fluorescence images of HEK cells coexpressing the plasma membrane marker and mRFP-tagged TPC2 in which Leu-11 and Leu-12 were replaced with Ala (TPC2$^{AA}$). *F*, epifluorescence (*Epi.*) and TIRF images of HEK cells expressing C-terminally GFP-tagged TPC2, TPC2ΔN, or TPC2$^{AA}$. Images (*D–F*) are typical examples from samples of 15–20 cells. All *scale bars*, 5 $\mu$m.

$\mu$l/cm$^2$ adherent cells) comprising 20 mM Tris (pH 7.2), 50 mM NaCl, 10 mM magnesium acetate, 1% Surfact-Amps X-100 (Pierce), and a EDTA-free protease inhibitor mixture (Roche Applied Sciences). The suspension was rotated for 60 min at 4 °C, then centrifuged (90,000 × *g*, 60 min, 4 °C), and the supernatant was incubated with or without peptide:*N*-glycosidase F (50,000 units/ml; New England Biolabs) for 60 min at 37 °C according to the manufacturer's instructions except that the denaturation step was omitted. Samples (10 $\mu$g) were resuspended in NuPAGE® LDS-sample buffer (Invitrogen) supplemented with 100 mM DTT and incubated at 20 °C for 60 min prior to SDS-PAGE using NuPAGE® Novex 4–12% BisTris gels (Invitrogen). Proteins were transferred to nitrocellulose, and Western blotting was performed as described in Ref. 20 using a mouse anti-GFP primary antibody (1:1000; Roche Applied Sciences) and an anti-mouse horseradish peroxidase-conjugated secondary antibody (1:1000; Invitrogen).

*Microscopy*—Confocal microscopy was performed as described previously (4). For TIRF microscopy, an Olympus IX81 microscope equipped with a 150×/1.45NA TIRF objective was used. Images

were acquired with an Andor iXON 897 camera (512 × 512 pixels). Cells were illuminated with either a 488-nm laser (TIRF) or a xenon arc lamp via a GFP (488-nm) filter set (widefield). All settings were identical for images of TPC2, TPC2ΔN, and TPC2$^{AA}$. Yellow-green FluoSpheres (100-nm diameter; Invitrogen) were used to establish the angle of reflection for TIRF.

*Cytosolic $Ca^{2+}$ Measurements*—Free cytosolic $Ca^{2+}$ concentrations of single fura-2-loaded SKBR3 cells were measured, and microinjection was performed as described (4). All microinjected cells were included in the analysis.

*Patch Clamp Recording*—The whole-cell or excised inside-out configurations were used for patch clamp recording at 20 °C from transiently transfected HEK cells (21). Unless stated otherwise, both bath and pipette solutions contained 200 mM $CsSO_3CH_3$, 2 mM CsCl, 10 mM HEPES (pH 7.2 with CsOH). For determination of the single-channel $Ca^{2+}$ conductance ($\gamma_{Ca}$), the solutions contained 140 mM calcium gluconate, 2 mM $CaCl_2$, 10 mM HEPES (pH 7.2 with CsOH). For determination of ionic selectivity, the solutions contained 140 mM NMDG gluconate, 2 mM NMDG-Cl, 10 mM HEPES (pH 7.2) with NMDG. The pipette tip resistance when filled with pipette

rected Mutagenesis kit (Stratagene) and mutagenic primers 5F and 5R. Constructs in which Leu-265 of GFP-tagged TPC2 or TPC2ΔN was replaced by Pro (TPC2$^{L265P}$ and TPC2ΔN$^{L265P}$) were generated similarly using mutagenic primers 6F and 6R. The coding sequences of all plasmids were fully sequenced to confirm that only the desired mutations were introduced.

*Cells and Transfection*—SKBR3 human breast cancer cells and HEK cells were cultured as described (4). For Western blot analyses, confocal microscopy, and patch clamp recording, cells were transiently transfected with plasmids using Lipofectamine$^{TM}$ 2000 transfection reagent (Invitrogen) according to the manufacturer's instructions. For total internal reflection fluorescence (TIRF) microscopy, cells were transfected using either the Neon transfection device (Invitrogen) for SKBR3 cells or by nucleofection (Amaxa) for HEK cells. Plasmid DNA was used at a concentration of 5 $\mu$g/100 $\mu$l of cells, and cells were then plated onto polylysine-coated glass-bottomed culture dishes (no. 0 coverglass; MatTek Corp.). Cells were used 1–2 days after transfection.

*Western Blotting*—Cells expressing GFP-tagged TPC2 constructs were harvested by scraping, washed by centrifugation (500 × *g*, 5 min), and resuspended in solubilization buffer (10

solution was 8–15 megohms (excised patch clamp recordings) and 5–8 megohms (whole-cell recordings). The methods used for recording and analyzing currents were reported previously (22). Briefly, currents were analyzed using the 50% threshold crossing criterion. Openings briefer than 700 $\mu$s (twice the filter rise time) were excluded from the analysis (23). Because it is difficult to establish the number of active channels when $P_o$ (the single-channel open probability) is low, we use $NP_o$ to report channel activity (22). Currents were filtered at 1 kHz and sampled at 10 kHz. For presentation only, traces were further filtered with a Gaussian digital filter at a cut-off frequency of 500 Hz.

*Materials*—NAADP, ryanodine, and cyclic ADP-ribose were from Sigma. Bafilomycin A$_1$ was from Calbiochem. *Trans*-NED19 was from Enzo Life Sciences.

## RESULTS AND DISCUSSION

*Targeting of TPC2 to Endo-lysosomes by a Dileucine Motif*—The N terminus of several mammalian TPCs includes a conserved dileucine-based motif (Fig. 1*B*). This sequence targets other trans-membrane proteins to endosomes and lysosomes (24). We expressed human TPC1 and TPC2 with and without their native N termini and used C-terminal mRFP or GFP tags to determine their subcellular distributions. After removal of the N terminus from TPC1 (TPC1ΔN), mutation of another dileucine motif near the C terminus (TPC1$^{AA}$) or combining both modifications (TPC1ΔN$^{AA}$), the expressed protein retained an intracellular distribution similar to that of TPC1 (supplemental Fig. S1). These results suggest that targeting of TPC1 does not require its dileucine motifs and may instead involve other sequences, possibly tyrosine-based motifs (24) that are also present in TPC1.

In contrast, TPC2ΔN localized to the plasma membrane although its level of expression and glycosylation were similar to those of TPC2 (Fig. 1*C* and supplemental Fig. S2*A*). In confocal images of SKBR3 breast cancer cells (Fig. 1*D*) and HEK cells (supplemental Fig. S2*B*), most TPC2ΔN was peripherally located and colocalized with a plasma membrane marker. The small amount of nonperipheral TPC2ΔN also colocalized with the plasma membrane marker (Fig. 1*D* and supplemental Fig. S2*B*), suggesting that it represents either TPC2ΔN in transit or invaginations of the plasma membrane. Similar plasma membrane targeting was obtained with TPC2 in which the dileucine motif was mutated by substitution of Leu-11 and Leu-12 with alanine (TPC2$^{AA}$, Fig. 1*E* and supplemental Fig. S2*C*). Additionally, despite similar levels of expression of TPC2, TPC2ΔN, and TPC2$^{AA}$ in HEK (Fig. 1*F*) and SKBR3 (supplemental Fig. S2*D*) cells determined using epifluorescence microscopy, TPC2ΔN and TPC2$^{AA}$ were much more evident within the plasma membrane region as revealed by TIRF microscopy. The small punctate TIRF signals from TPC2-expressing cells (Fig. 1*F* and supplemental Fig. S2*D*) probably arise from TPC2 in lysosomes lying within 100 nm of the plasma membrane, consistent with our detection of similar signals from cells labeled with Lysotracker Red (data not shown). Together, these results demonstrate that loss of the N-terminal dileucine motif prevents the normal trafficking of TPC2 to lysosomes. TPC2ΔN and TPC2$^{AA}$ are instead localized at the plasma membrane.

Mouse TPC2 has been reported to remain intracellular after deletion of its N terminus (3), suggesting either that this truncated protein was misfolded or that mouse TPC2 has an additional lysosomal targeting motif.

*Uncoupling of NAADP-evoked Ca$^{2+}$ Signals from Activation of Ryanodine Receptors*—We measured cytosolic Ca$^{2+}$ signals after microinjection of NAADP into fura-2-loaded SKBR3 cells transiently transfected with plasmids encoding TPC2. NAADP increased the cytosolic Ca$^{2+}$ concentration in cells expressing TPC2 (Fig. 2*A* and supplemental Fig. S3*A*), but not in GFP-transfected cells, nor was there any response from TPC2-expressing cells microinjected with buffer (Fig. 2*B*). The latter demonstrates that responses to microinjected NAADP are not, as some have suggested (6), a consequence of TPC2 causing increased mechanosensitivity. The selective NAADP antagonist, *trans*-NED19 (25), blocked the Ca$^{2+}$ signals evoked by microinjected NAADP (Fig. 2*B*), further demonstrating the specificity of the NAADP-evoked Ca$^{2+}$ signals in TPC2-expressing cells.

In cells expressing TPC2, the peak Ca$^{2+}$ signals evoked by NAADP were substantially inhibited after treatment with ryanodine (Fig. 2*C*), indicating a requirement for ryanodine receptors, which are expressed in the ER. The responses were abolished after treatment with bafilomycin A$_1$, an inhibitor of V-type ATPases, confirming the involvement of acidic organelles (Fig. 2*C*). These results show that NAADP mobilizes Ca$^{2+}$ from intracellular Ca$^{2+}$ stores and involves activation of both TPC2 and ryanodine receptors.

In similar experiments with cells expressing TPC2ΔN, microinjection of NAADP, but not buffer, also evoked Ca$^{2+}$ signals (Fig. 2, *A* and *B*, and supplemental Fig. S3*B*), and these too were abolished by *trans*-NED19 (Fig. 2*B*). In contrast to the results with TPC2, ryanodine had no effect on the amplitude of the Ca$^{2+}$ signals in TPC2ΔN-expressing cells, although the rising phase of the response was slightly slower (Fig. 2*D*). Bafilomycin A$_1$, which abolished responses to NAADP in TPC2-expressing cells, modestly enhanced responses to NAADP in TPC2ΔN-expressing cells (Fig. 2*D*), perhaps reflecting the reduced ability of acidic stores to sequester Ca$^{2+}$ (discussed in Ref. 26). Furthermore, the Ca$^{2+}$ signals evoked by NAADP in TPC2ΔN-expressing cells were abolished by removal of extracellular Ca$^{2+}$ whereas they persisted in TPC2-expressing cells (Fig. 2*E*). Although even in the latter, responses to NAADP were attenuated, probably because the associated stimulation of ryanodine receptors depletes the ER of Ca$^{2+}$ and thereby normally stimulates store-operated Ca$^{2+}$ entry. These results demonstrate that TPC2ΔN mediates NAADP-evoked Ca$^{2+}$ entry, consistent with its plasma membrane distribution (Fig. 1, *D–F*, and supplemental Fig. S2, *B–D*). Together, these results (supplemental Fig. S4, *A–C*) show that targeting of TPC2 to the plasma membrane dissociates activation of TPC2 from activation of ryanodine receptors. This uncoupling is not caused by impaired function of ryanodine receptors because responses to cyclic ADP-ribose, which activates ryanodine receptors (27), were similar in cells expressing TPC2 and TPC2ΔN (Fig. 2*F* and supplemental Fig. S4*C*). We conclude that inhibition of NAADP-evoked Ca$^{2+}$ signals by ryanodine in cells expressing TPC2 (Fig. 2*C*) results from disruption of an amplification
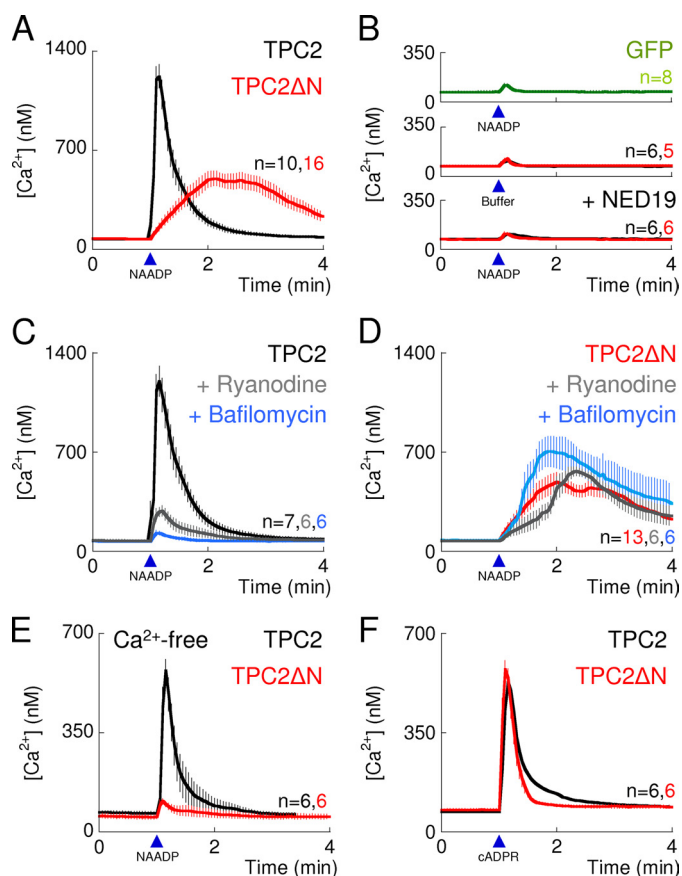
FIGURE 2. **TPC2 targeted to the plasma membrane is uncoupled from ryanodine receptors.** *A–F*, cytosolic Ca$^{2+}$ signals from individual fura-2-loaded SKBR3 cells transiently transfected with C-terminally GFP-tagged TPC2 (*black traces*), TPC2ΔN (*red traces*), or GFP alone (*green*). *A* and *B*, responses to microinjection (*arrowheads*) with NAADP (10 nm) or buffer. Cells were incubated with *trans*-NED19 (100 nm, 15 min) as indicated. *C* and *D*, responses to microinjection of NAADP (10 nm) from untreated cells or cells incubated with ryanodine (10 μm, 15 min) or bafilomycin A$_1$ (1 μm, 60 min) as indicated. *E*, extracellular Ca$^{2+}$ was removed 2–3 min before injection of NAADP. *F*, cells injected with cyclic ADP-ribose (*cADPR*, 500 nm). Results are means ± S.E. of the indicated number (*n*) of cells.

pathway rather than a direct effect of NAADP on ryanodine receptors. Other Ca$^{2+}$-permeable channels can also amplify NAADP-evoked Ca$^{2+}$ signals, for example inositol trisphosphate receptors in HEK cells (2) or nonselective cation channels in medulla neurons (28). The lack of such amplification in TPC2ΔN-expressing cells probably explains the smaller amplitude and modestly slower rise times of their NAADP-evoked Ca$^{2+}$ signals (Fig. 2*A* and supplemental Fig. S4*D*), although we note that in TPC2-expressing cells (Fig. 2*B*), ryanodine appeared to affect only the amplitude of the Ca$^{2+}$ signals. Differences in the pH and/or Ca$^{2+}$ concentration of the extracellular medium compared with the lumen of the lysosome may also contribute to the different kinetics.

*Single-channel Properties of TPC2*—Targeting of functional TPC2 to the plasma membrane provided the first opportunity to examine its single-channel behavior in a native membrane. In whole-cell recordings from HEK cells expressing TPC2ΔN and using Cs$^+$ as the charge-carrier, intracellular NAADP (500 nm) evoked currents that were slightly inwardly rectifying (Fig. 3, *A* and *B*). We detected no such currents in either control cells or in cells expressing full-length TPC2 (Fig. 3*A*). In media con-
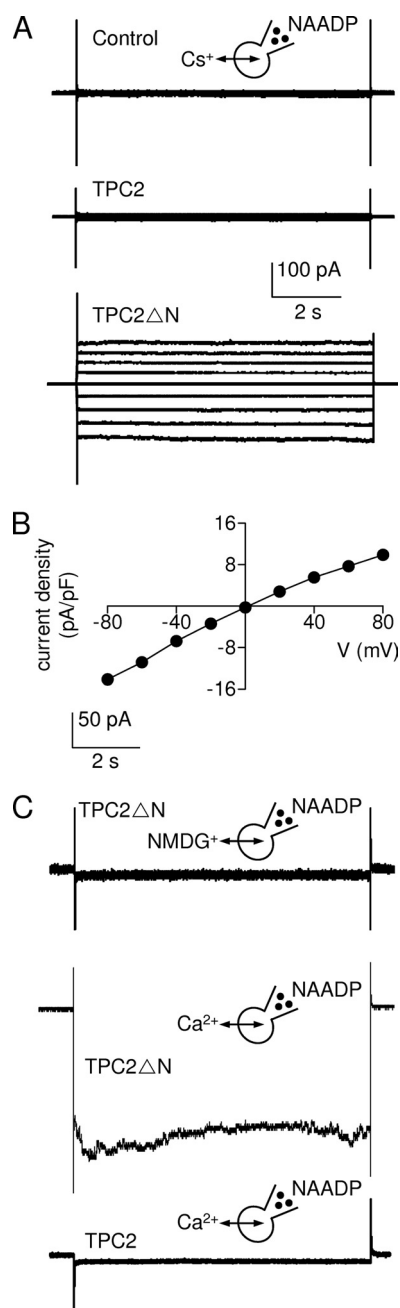


FIGURE 3. **TPC2 is an NAADP-gated Ca$^{2+}$-permeable cation channel.** *A*, whole-cell recordings were performed from nontransfected HEK cells or after transient transfection with C-terminally GFP-tagged TPC2 or TPC2ΔN. With 500 nm NAADP in the pipette solution, and from a holding potential of 0 mV, the potential was switched in 20-mV increments from −80 to +80 mV, and the whole-cell currents were recorded. Results typical of 8 experiments are shown. *B*, from experiments similar to those in *A*, the current density-voltage (*V*) relationship for the NAADP-activated whole-cell current is shown. Results are means ± S.E., *n* = 6 (*error bars* are smaller than the *symbols*). *C*, whole-cell recordings are similar to those shown in *A*, but using either symmetrical Ca$^{2+}$ gluconate or NMDG gluconate-based solutions as indicated. With 500 nm NAADP in the pipette solution, the inward whole-cell current was recorded in response to stepping to −140 mV from a holding potential of 0 mV. Results typical of five or three (*middle trace*) experiments are shown.

taining symmetrical calcium gluconate, NAADP evoked whole-cell currents in cells expressing TPC2ΔN, but not in those expressing TPC2 (Fig. 3*C*). There were no currents in the TPC2ΔN-expressing cells when the Ca$^{2+}$ was replaced with an
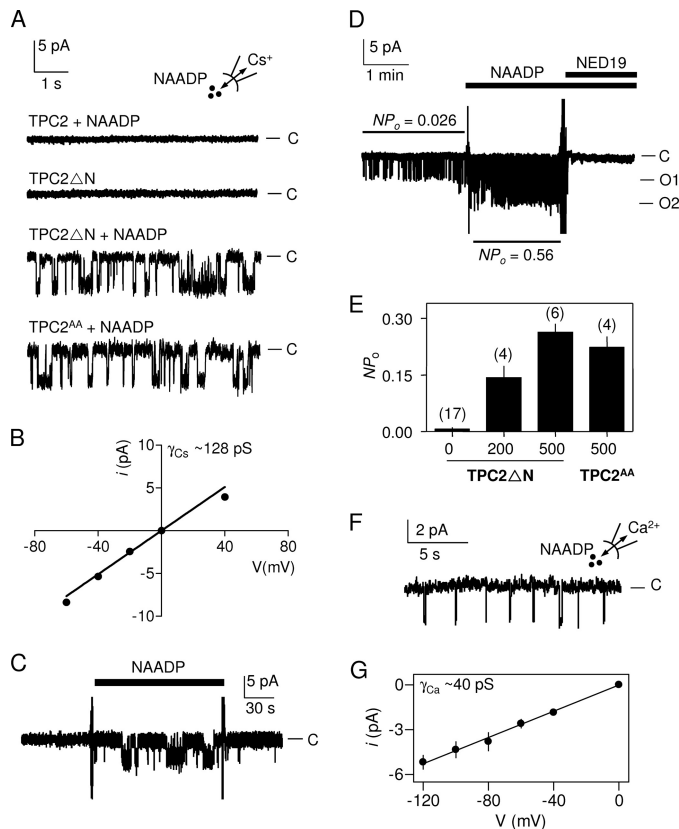
**FIGURE 4. Activation of single $Ca^{2+}$-permeable TPC2 channels by NAADP.** *A*, typical recordings from excised inside-out patches from the plasma membrane of HEK cells expressing TPC2, TPC2$\Delta$N, or TPC2$^{AA}$ and stimulated as indicated with NAADP (500 nM in the bathing solution). $Cs^+$ was the charge carrier, and the holding potential was $-60$ mV; *C* denotes the closed state. Results are typical (from *top* to *bottom*) of 15, 17, 17, and 4 experiments, respectively. *B*, current (*i*)-voltage (*V*) relationship for the NAADP-activated channels in TPC2$\Delta$N-expressing cells. Results are means $\pm$ S.E., $n = 8$. *C*, recording, typical of three experiments, from an excised inside-out patch from the plasma membrane of HEK cells expressing TPC2$\Delta$N. NAADP (500 nM) was added and removed as indicated. *C* denotes the closed state. *D*, recording, typical of three similar records, from a patch excised from the plasma membrane of HEK cells expressing TPC2$\Delta$N and treated with NAADP (500 nM) and *trans*-NED19 (100 nM) as indicated. $Cs^+$ was the charge carrier, and the holding potential was $-40$ mV; *C*, *O1*, and *O2* denote the closed state and openings of one and two channels, respectively. Note the presence of basal activity ($NP_o$), which is increased $\sim$20-fold by the addition of NAADP; *trans*-NED19 inhibits both the basal and NAADP-evoked activity. In both *C* and *D* changes of media are accompanied by brief electrical spike artifacts. *E*, summary results showing $NP_o$ for excised patches of cells expressing TPC2$\Delta$N or TPC2$^{AA}$ and stimulated with the indicated concentrations of NAADP (nanomolar) in the bathing solution. Results are means $\pm$ S.E., with *n* shown above each *bar*. *F*, record, typical of five similar records, from an excised patch expressing TPC2$\Delta$N and with $Ca^{2+}$ as the charge carrier. Pipette solution contained 500 nM NAADP, and the holding potential was $-110$ mV. *C* denotes the closed state. *G*, current-voltage relationship from records similar to those shown in *F*. Recordings were restricted to negative holding potentials to avoid activation of voltage-gated $Ca^{2+}$ channels that may be endogenously expressed in HEK cells (34). Results are means $\pm$ S.E., $n = 5$.

impermeant cation (NMDG$^+$) (Fig. 3*C*). These results demonstrate that NAADP activates a $Ca^{2+}$-permeable cation channel in the plasma membrane of cells expressing TPC2$\Delta$N.

In 17 of 38 recordings from inside-out patches from the plasma membrane of cells expressing TPC2$\Delta$N, NAADP (200–500 nM, in the bathing solution) stimulated bursts of channel openings (Fig. 4*A*). Detection of channels in $\sim$40% of patches suggests an average of $\sim$0.5 randomly distributed channels/patch and is consistent with the relative scarcity ($\sim$8%) of patches in

which we detected more than one channel (supplemental text). The current-voltage relationship for these single-channel openings was, like the whole-cell currents (Fig. 3*B*), slightly inwardly rectifying. The unitary $Cs^+$ conductance ($\gamma_{Cs}$, measured between 0 and $-60$ mV) was $128 \pm 4$ pS (Fig. 4*B*). In continuous recordings, NAADP rapidly and reversibly stimulated this channel activity (Fig. 4*C*), and *trans*-NED19 rapidly reversed the activity (Fig. 4*D*). Channels with indistinguishable conductance ($\gamma_{Cs} = 138 \pm 15$ pS, $n = 4$, data not shown) and $NP_o$ (Fig. 4, *A* and *E*) were detected in excised patches from cells expressing TPC2$^{AA}$. We detected no such channels in parallel recordings from either mock-transfected cells ($n = 20$; data not shown) or from cells expressing TPC2 (Fig. 4*A*). Some patches from TPC2$\Delta$N-expressing cells (3 of 17 recordings) had detectable activity in the absence of added NAADP, although most were quiescent. In each, the activity was massively increased by addition of 200 or 500 nM NAADP (Fig. 4*E*).

*TPC2 is a Pore-forming Subunit of the $Ca^{2+}$-permeable NAADP-activated Channel*—To determine the $Ca^{2+}$ permeability of the NAADP-activated channel, we recorded currents in excised patches from TPC2$\Delta$N-expressing cells in symmetrical $Ca^{2+}$ at negative holding potentials (Fig. 4*F*). From the slopes of the linear current-voltage relationships, the unitary $Ca^{2+}$ conductance ($\gamma_{Ca}$) of the NAADP-activated channel was $40 \pm 1.3$ pS (Fig. 4*G*). NAADP did not activate $Ca^{2+}$-permeable channels in cells expressing full-length TPC2 ($n = 8$; data not shown). We note that whereas bursts of openings are common with $Cs^+$ as the charge carrier (Fig. 2, *A*, *C*, and *D*), they are less common with $Ca^{2+}$ as the charge carrier (Fig. 4*F* and supplemental Fig. S5). Such effects of permeating ions on channel gating kinetics are also observed for other channels (29–31). These results establish that TPC2 is an essential component of the $Ca^{2+}$-permeable cation channel activated by NAADP.

An outstanding question is whether TPC2 is itself the pore-forming subunit of the channel. To address this issue, we mutated a conserved residue (Leu-265) within a putative pore region (4) of TPC2 and TPC2$\Delta$N (Fig. 5*A*). The mutant, TPC2$^{L265P}$, showed an intracellular distribution similar to that of TPC2, whereas TPC2$\Delta$N$^{L265P}$, like TPC2$\Delta$N, localized to the plasma membrane in both SKBR3 (Fig. 5*B*) and HEK (supplemental Fig. S2*E*) cells. Microinjection of NAADP into SKBR3 cells expressing either TPC2$^{L265P}$ or TPC2$\Delta$N$^{L265P}$ failed to evoke $Ca^{2+}$ signals (Fig. 5*C*). We recorded $Cs^+$ currents in excised patches from cells expressing TPC2$\Delta$N$^{L265P}$. NAADP (500 nM) activated channels in these patches (Fig. 5*D*) that had similar activity ($NP_o = 0.32 \pm 0.04$, $n = 3$) to those of TPC2$\Delta$N, but their $\gamma_{Cs}$ was massively reduced to $9.5 \pm 0.41$ pS (Fig. 5*E*). These results, showing that a mutation within the putative pore of TPC2 affects the conductance of the NAADP-activated channel, establish that TPC2 is a pore-forming subunit of the NAADP-activated cation channel. While our work was under review, others reported NAADP-evoked $Ca^{2+}$ currents from enlarged lysosomes of cells overexpressing mouse TPC2 (32) and single-channel recordings from immunopurified human TPC2 incorporated into artificial lipid bilayers (33). Both studies reported dramatic effects of luminal pH on channel activity (32, 33). Our study is consistent with that of Pitt *et al.* (33) in demonstrating NAADP-stimulated channel activity at neutral
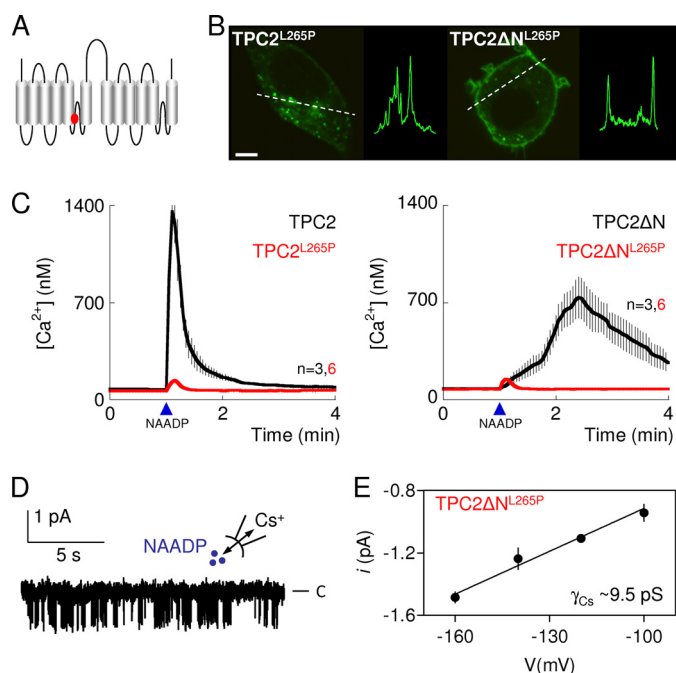
FIGURE 5. **TPC2 is the pore-forming subunit of an NAADP-gated channel.** *A*, depiction of TPC2 showing location of a putative pore residue (Leu-265, *red*). *B*, confocal fluorescence images of SKBR3 cells expressing GFP-tagged TPC2 in which Leu-265 was replaced by proline (TPC2$^{L265P}$, *left*) or in which this was combined with removal of the N terminus (TPC2$\Delta$N$^{L265P}$, *right*). Images are typical of those from 6–10 cells. *Scale bar*, 5 $\mu$m. Similar results with HEK cells are shown in supplemental Fig. S2E. *C*, cytosolic Ca$^{2+}$ signals from individual fura-2-loaded SKBR3 cells transiently transfected with the indicated C-terminally GFP-tagged TPC2 constructs and microinjected with NAADP (10 nM, *arrowheads*). Results are means ± S.E. of the indicated number (*n*) of cells. *D*, recording, typical of four similar records, from excised inside-out patches from the plasma membrane of HEK cells expressing TPC2$\Delta$N$^{L265P}$ and stimulated with 500 nM NAADP in the bathing solution with Cs$^+$ as the charge carrier. *C* denotes the closed state. *E*, current-voltage relationship from records similar to those shown in *D*. Results are means ± S.E., *n* = 4.

pH, although in our experiments the effects of NAADP were more rapid in onset, reversible, and blocked by lower concentrations of *trans*-NED19. Our results and those from Pitt *et al.* (33) differ, however, from the study of Scheider *et al.* (32), who detected NAADP-mediated currents only at acidic luminal pH.

## CONCLUSIONS

By manipulating an endogenous endo-lysosomal targeting sequence near the N terminus of TPC2, we succeeded in expressing TPC2 in the plasma membrane. This allowed us to dissociate activation of TPC2 by NAADP from amplification of the initial Ca$^{2+}$ signal by Ca$^{2+}$ release from the ER, thereby demonstrating that ryanodine receptors are not the primary targets of NAADP. Our single-channel recordings and mutagenesis demonstrate that TPC2 is a pore-forming subunit of a Ca$^{2+}$-permeable channel activated by NAADP.

## REFERENCES

1. Guse, A. H., and Lee, H. C. (2008) *Sci. Signal.* **1,** re10
2. Calcraft, P. J., Ruas, M., Pan, Z., Cheng, X., Arredouani, A., Hao, X., Tang, J., Rietdorf, K., Teboul, L., Chuang, K. T., Lin, P., Xiao, R., Wang, C., Zhu, Y., Lin, Y., Wyatt, C. N., Parrington, J., Ma, J., Evans, A. M., Galione, A., and Zhu, M. X. (2009) *Nature* **459,** 596–600
3. Zong, X., Schieder, M., Cuny, H., Fenske, S., Gruner, C., Rötzer, K., Griesbeck, O., Harz, H., Biel, M., and Wahl-Schott, C. (2009) *Pflugers Arch.* **458,** 891–899
4. Brailoiu, E., Churamani, D., Cai, X., Schrlau, M. G., Brailoiu, G. C., Gao, X., Hooper, R., Boulware, M. J., Dun, N. J., Marchant, J. S., and Patel, S. (2009) *J. Cell Biol.* **186,** 201–209
5. Brailoiu, E., Hooper, R., Cai, X., Brailoiu, G. C., Keebler, M. V., Dun, N. J., Marchant, J. S., and Patel, S. (2010) *J. Biol. Chem.* **285,** 2897–2901
6. Ruas, M., Rietdorf, K., Arredouani, A., Davis, L. C., Lloyd-Evans, E., Koegel, H., Funnell, T. M., Morgan, A. J., Ward, J. A., Watanabe, K., Cheng, X., Churchill, G. C., Zhu, M. X., Platt, F. M., Wessel, G. M., Parrington, J., and Galione, A. (2010) *Curr. Biol.* **20,** 703–709
7. Patel, S., Marchant, J. S., and Brailoiu, E. (2010) *Cell Calcium* **47,** 480–490
8. Churchill, G. C., Okada, Y., Thomas, J. M., Genazzani, A. A., Patel, S., and Galione, A. (2002) *Cell* **111,** 703–708
9. Mitchell, K. J., Lai, F. A., and Rutter, G. A. (2003) *J. Biol. Chem.* **278,** 11057–11064
10. Yamasaki, M., Masgrau, R., Morgan, A. J., Churchill, G. C., Patel, S., Ashcroft, S. J., and Galione, A. (2004) *J. Biol. Chem.* **279,** 7234–7240
11. Kinnear, N. P., Boittin, F. X., Thomas, J. M., Galione, A., and Evans, A. M. (2004) *J. Biol. Chem.* **279,** 54319–54326
12. Brailoiu, E., Hoard, J. L., Filipeanu, C. M., Brailoiu, G. C., Dun, S. L., Patel, S., and Dun, N. J. (2005) *J. Biol. Chem.* **280,** 5646–5650
13. Cancela, J. M., Churchill, G. C., and Galione, A. (1999) *Nature* **398,** 74–76
14. Churchill, G. C., and Galione, A. (2001) *EMBO J.* **20,** 2666–2671
15. Gerasimenko, J. V., Maruyama, Y., Yano, K., Dolman, N. J., Tepikin, A. V., Petersen, O. H., and Gerasimenko, O. V. (2003) *J. Cell Biol.* **163,** 271–282
16. Langhorst, M. F., Schwarzmann, N., and Guse, A. H. (2004) *Cell. Signal.* **16,** 1283–1289
17. Mojzisová, A., Krizanová, O., Záciková, L., Komínková, V., and Ondrias, K. (2001) *Pflugers Arch.* **441,** 674–677
18. Hohenegger, M., Suko, J., Gscheidlinger, R., Drobny, H., and Zidar, A. (2002) *Biochem. J.* **367,** 423–431
19. Dammermann, W., Zhang, B., Nebel, M., Cordiglieri, C., Odoardi, F., Kirchberger, T., Kawakami, N., Dowden, J., Schmid, F., Dornmair, K., Hohenegger, M., Flügel, A., Guse, A. H., and Potter, B. V. (2009) *Proc. Natl. Acad. Sci. U.S.A.* **106,** 10678–10683
20. Churamani, D., Boulware, M. J., Geach, T. J., Martin, A. C., Moy, G. W., Su, Y. H., Vacquier, V. D., Marchant, J. S., Dale, L., and Patel, S. (2007) *PLoS ONE* **2,** e797
21. Hamill, O. P., Marty, A., Neher, E., Sakmann, B., and Sigworth, F. J. (1981) *Pflugers Arch.* **391,** 85–100
22. Taufiq-Ur-Rahman, Skupin, A., Falcke, M., and Taylor, C. W. (2009) *Nature* **458,** 655–659
23. Sakmann, B., and Neher, E. (1995) *Single-Channel Recording*, 2nd Ed., Plenum Press, New York
24. Bonifacino, J. S., and Traub, L. M. (2003) *Annu. Rev. Biochem.* **72,** 395–447
25. Naylor, E., Arredouani, A., Vasudevan, S. R., Lewis, A. M., Parkesh, R., Mizote, A., Rosen, D., Thomas, J. M., Izumi, M., Ganesan, A., Galione, A., and Churchill, G. C. (2009) *Nat. Chem. Biol.* **5,** 220–226
26. Patel, S., and Docampo, R. (2010) *Trends Cell Biol.* **20,** 277–286
27. Galione, A., and Churchill, G. C. (2000) *Sci. STKE* **2000,** pe1
28. Brailoiu, G. C., Brailoiu, E., Parkesh, R., Galione, A., Churchill, G. C., Patel, S., and Dun, N. J. (2009) *Biochem. J.* **419,** 91–97
29. Bezprozvanny, I., and Ehrlich, B. E. (1994) *J. Gen. Physiol.* **104,** 821–856
30. Lu, T., Wu, L., Xiao, J., and Yang, J. (2001) *J. Gen. Physiol.* **118,** 509–522
31. Kusch, J., Nache, V., and Benndorf, K. (2004) *J. Physiol* **560,** 605–616
32. Schieder, M., Rötzer, K., Brüggemann, A., Biel, M., and Wahl-Schott, C. A. (2010) *J. Biol. Chem.* **285,** 21219–21222
33. Pitt, S. J., Funnell, T., Sitsapesan, M., Venturi, E., Rietdorf, K., Ruas, M., Ganesan, A., Gosain, R., Churchill, G. C., Zhu, M. X., Parrington, J., Galione, A., and Sitsapesan, R. (2010) *J. Biol. Chem.* **285,** in press
34. Thomas, P., and Smart, T. G. (2005) *J. Pharmacol. Toxicol. Methods* **51,** 187–200